JGR Atmospheres

RESEARCH ARTICLE
10.1029/2020JD034047

Special Section:
Water-energy-carbon fluxes over terrestrial water surfaces

How Land-Sea Interaction of Tidal and Sea Breeze Activity Affect Mangrove Net Ecosystem Exchange?

Xudong Zhu[1,2], Zhangcai Qin[2,3], and Lulu Song[4]

[1]State Key Laboratory of Marine Environment Science, Taiwan Strait Marine Ecosystem National Observation and Research Station, Key Laboratory of the Coastal and Wetland Ecosystems (Ministry of Education), Coastal and Ocean Management Institute, College of the Environment and Ecology, Xiamen University, Xiamen, Fujian, China, [2]Southern Marine Science and Engineering Guangdong Laboratory (Zhuhai), Zhuhai, Guangdong, China, [3]School of Atmospheric Sciences, Guangdong Province Key Laboratory for Climate Change and Natural Disaster Studies, Sun Yat-sen University, Zhuhai, Guangdong, China, [4]Key Laboratory of Urban Environment and Health, Institute of Urban Environment, Chinese Academy of Sciences, Xiamen, Fujian, China

Abstract Coastal mangrove wetlands experience unique land-sea interaction including periodic tidal and sea breeze activity; however, their impacts on mangrove net ecosystem exchange (NEE) of carbon dioxide have not been well investigated. In this regard, continuous eddy covariance and auxiliary measurements were conducted to characterize the temporal variations in NEE and environmental controls in a subtropical mangrove of southeastern China. Over a 3-year measurement period, this mangrove acted a consistent carbon sink showing weak seasonality in NEE with a stronger sink in spring. Environmental controls on NEE varied across time scales: (1) at half-hourly time scale especially for summer and autumn, high temperature and vapor pressure deficit (VPD) suppressed daytime carbon uptake, while inundation fraction and rain restrained nighttime carbon efflux; (2) the importance of environmental impacts on daily NEE decreased in the order of photosynthetically active radiation, air temperature, sea breeze, VPD, tidal salinity, and inundation; (3) monthly carbon uptake was statistically negatively and positively correlated with inundation fraction and rain, respectively. Periodic tidal inundation exerted both direct and indirect effects, but their relative importance changed across time scales. Cooling and wetting effects from regular sea breeze relieved atmospheric temperature/moisture stresses at afternoon, acting as an important indirect effect to promote carbon uptake. This study confirms the importance of previously neglected indirect effects of land-sea interaction of tidal and sea breeze activity on mangrove NEE.

Key Points:

- Periodic tidal inundation exerted both direct and indirect effects on mangrove net ecosystem exchange
- Regular sea breeze relieved atmospheric temperature/moisture stresses and enhanced mangrove carbon uptake
- Previously neglected indirect effects of land-sea interaction on mangrove carbon flux were important

Supporting Information:

Supporting Information may be found in the online version of this article.

Correspondence to:

X. Zhu and L. Song,
xdzhu@xmu.edu.cn;
llsong@iue.ac.cn

Citation:

Zhu, X., Qin, Z., & Song, L. (2021). How land-sea interaction of tidal and sea breeze activity affect mangrove net ecosystem exchange? *Journal of Geophysical Research: Atmospheres*, *126*, e2020JD034047. https://doi.org/10.1029/2020JD034047

Received 7 OCT 2020
Accepted 4 APR 2021

Author Contributions:

Conceptualization: Zhangcai Qin
Formal analysis: Zhangcai Qin
Investigation: Lulu Song
Methodology: Lulu Song
Validation: Lulu Song
Visualization: Lulu Song
Writing – original draft: Zhangcai Qin, Lulu Song
Writing – review & editing: Zhangcai Qin

1. Introduction

As one of the most important blue carbon ecosystems (Nellemann & Corcoran, 2009), tidal mangroves contain rich carbon storage and sequestrate atmospheric carbon dioxide (CO_2) at much larger rates per unit area than inland forests (Alongi, 2014; Mcleod et al., 2011). With high carbon sink potential, mangroves have been increasingly recognized as an effective long-term carbon sink option in climate change mitigation (Howard et al., 2017). To conduct a scientific assessment of mitigation potential, detailed characterization of mangrove carbon fluxes and accurate quantification of mangrove carbon budgets are needed. However, the knowledge of temporal and spatial variations in mangrove carbon fluxes and their responses to environmental factors are very limited (Alongi, 2012). On the one hand, located in the margin between land and sea, mangrove carbon fluxes are subject to many other environmental stresses except for those typically with inland forests, such as tidal inundation (Crase et al., 2015), high salinity (Song et al., 2011) and wastewater pollution (Jiang et al., 2018). On the other hand, it is challenging to manually monitor mangrove carbon fluxes on a regular basis due to notoriously difficult field conditions and inaccessibility to mangrove forests.

The magnitude of mangrove carbon fluxes can be estimated indirectly by stock-difference methods and directly by flux methods (Howard et al., 2014). The stock-difference methods calculate the change in carbon stock between two points in time and use the change as a proxy of carbon fluxes, while flux methods directly measure gaseous carbon fluxes using gas flux techniques including static chamber and eddy covariance (EC). Static chamber method is the most common gas flux technique to calculate gaseous carbon fluxes, but this method suffers from several issues, such as chamber-induced change in temperature/light during the

measurements and spatial/temporal misrepresentation of measured fluxes. To overcome these issues, the nondestructive EC technique (Baldocchi et al., 2001) has been used to provide a long-term, continuous, and near-direct measurements of net ecosystem CO_2 exchange (NEE) between ecosystem and the atmosphere, despite of the fact that the reliability of EC-based NEE suffers from suboptimal terrain/instrument setups and insufficient turbulent mixing. With continuous EC measurements, the temporal variations in NEE and its response to various environmental factors can be better characterized. Although EC measurements have been made over 900 sites (registered as FLUXNET sites) across a variety of ecosystems over the past two decades (Chu et al., 2017), the EC applications in tidal mangrove ecosystems are limited to only a few sites (Barr et al., 2010; Cui et al., 2018; Leopold et al., 2016; Liu & Lai, 2019). These EC studies have greatly improved our understanding of mangrove carbon cycles, but there is still a paucity of mangrove EC measurements given that mangrove NEE is temporally varying and spatially heterogeneous across complex and diversified intertidal habitats (Alongi, 2012; 2014).

Mangrove NEE is the net balance of CO_2 influx via gross primary productivity (GPP), CO_2 efflux via ecosystem respiration (Re) and lateral export of inorganic and organic carbon via tidal activity, and thus the magnitude of mangrove NEE is affected by environmental factors that regulate these processes. As with inland forests, mangrove GPP and Re processes are controlled by meteorological factors such as temperature, photosynthetically active radiation (PAR), and vapor pressure deficit (VPD). Temperature is the dominant factor of determining spatial distribution and growth of mangroves at global scale (Friess et al., 2019; Osland et al., 2017), and cold stresses are often reported to constrain mangrove growth and its photosynthetic capacity (Chen et al., 2017; Malone et al., 2016). Different from inland forests where soil respiration is generally co-limited by temperature and moisture (Hursh et al., 2017), mangrove soil respiration is presumably more affected by temperature since soil tends to be consistently wet. PAR exerts more significant effects on GPP in mangroves than inland forests (Barr, Engel, et al., 2013; Cui et al., 2018; Liu & Lai, 2019), because coastal mangroves usually experience more variable light intensity with frequent cloud/rain formations. The down-regulation of high VPD on GPP is widely observed due to reduced stomatal conductance under strong atmospheric vapor stress in many ecosystems (Novick et al., 2016) including mangroves (Leopold et al., 2016; Liu & Lai, 2019).

In addition to meteorological factors, coastal mangrove forests also experience unique land-sea interaction including periodic tidal activity and wind regimes, which could make the magnitude, temporal variation and its controls of mangrove NEE rather different from inland forests (Figure 1). Tides directly and indirectly affect mangrove NEE via different ways. Here, direct effects of tidal activities on mangrove NEE refer to anoxia effect from tidal inundation and export effect from tidal currents, while indirect effects of tidal activities refer to cooling/warming effect due to thermal contrasts between tidal waters and air/soils. For one thing (in terms of direct effects), mangrove soils become more saturated with tidal inundation, and thus less CO_2 is produced through ecosystem respiration under anoxia conditions (Alongi, 2009) (anoxia effect). With tidal inundation acting a barrier of gas transport, a portion of produced CO_2 has been exported horizontally via tidal activity in the form of dissolved inorganic carbon (Alongi, 2014) (export effect). Anoxia and export effects of tidal cycles suppress the strength of Re and subsequent CO_2 efflux, respectively. For another (in terms of indirect effects), with temperature gradients between tidal floodwaters and underlying soils and overlying atmosphere, tidal inundation indirectly affect ecosystem respiration and photosynthesis since tidal floodwaters function as a heat capacitor to adjust air/soil temperature (Barr, Fuentes, et al., 2013; Moffett et al., 2010): tidal floodwaters serve as a sink of energy at afternoon with positive air-water temperature gradients (cooling effect), but could shift to a net source of energy at nighttime/morning with opposite gradients (warming effect). Previous studies have examined tidal impacts on mangrove NEE (Barr et al., 2010; Q. Li et al., 2014; Liu & Lai, 2019), but they mostly focused on direct effects with indirect effects being less studied.

In comparison with tidal effects, the influence of wind regimes on carbon cycle in coastal ecosystems received even less attention (Huang et al., 2019). Due to the differences in surface air pressure created by contrasting radiation heating between land and sea, a sea breeze or onshore wind usually develops in coastal region at daytime especially in the afternoon. By contrast, a land breeze or offshore wind usually develops at nighttime or early morning due to the reverse effect. Daytime coastal meteorological conditions are frequently modified by sea breeze that brings in cooler and wetter air from the sea than that in the land (Miller

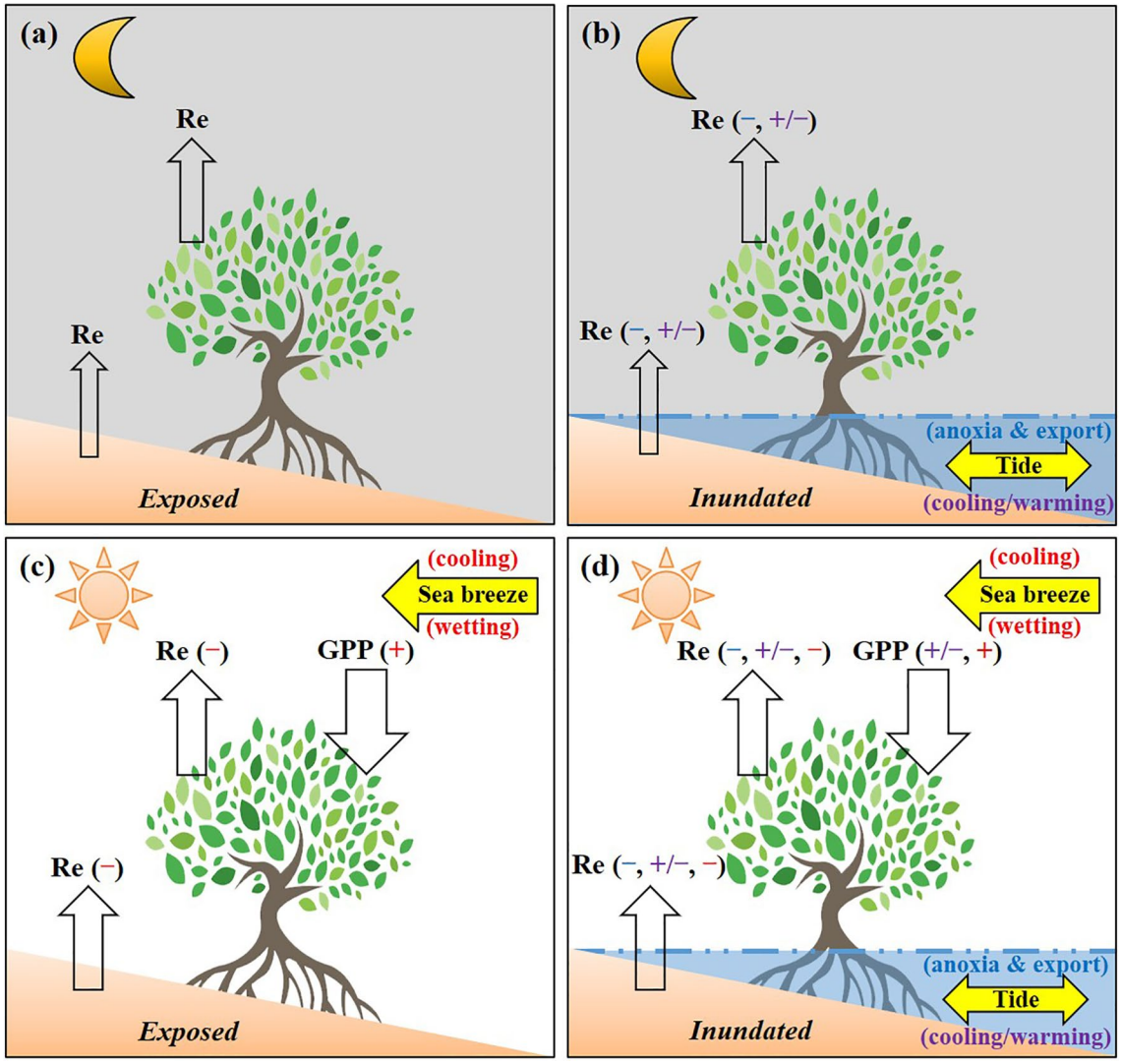

Figure 1. Conceptual diagrams illustrating the effects of land-sea interaction of tidal and sea breeze activity on mangrove carbon fluxes at nighttime (upper panel) and daytime (lower panel) under exposed (left panel) and inundated (right panel) conditions. GPP: gross primary productivity; Re: ecosystem respiration. Negative and positive signs in brackets denote corresponding effects of tidal or sea breeze activity on GPP and Re. See main text for more details.

et al., 2003). Therefore, in addition to potential direct effects due to the change in wind speed (e.g., affect flux footprint of the EC system), the magnitude and timing of sea breeze could also affect mangrove NEE indirectly by adjusting air temperature (cooling effect) and VPD (wetting effect), which are key environmental controls in regulating GPP or Re (Figure 1). Cooling and wetting effects of sea breeze relieve atmospheric stresses of high temperature and high VPD, respectively, which in turn reduces Re and promotes GPP. In addition, the formation and development of sea breeze are also affected by tidal activity via two processes (Fischereit et al., 2016): (1) the dynamic influence of tidal currents on surface wind speed and (2) the thermal influence of flooding and drying of intertidal mudflats. Furthermore, the timing of tidal activity and sea breeze are out of sync since they follow the lunar cycle and the solar cycle, respectively. This makes it more complicated to examine potential contributions of tidal activity, sea breeze and their interaction to mangrove NEE.

As far as we know, there is no such a study focusing on assessing direct and indirect impacts of tidal and sea breeze activity on carbon fluxes in mangrove ecosystems. A thorough analysis using continuous EC measurements could help close this knowledge gap. In this study, we focused on examining the effects of environmental controls on mangrove NEE with an emphasis on tidal and sea breeze activity, based on a

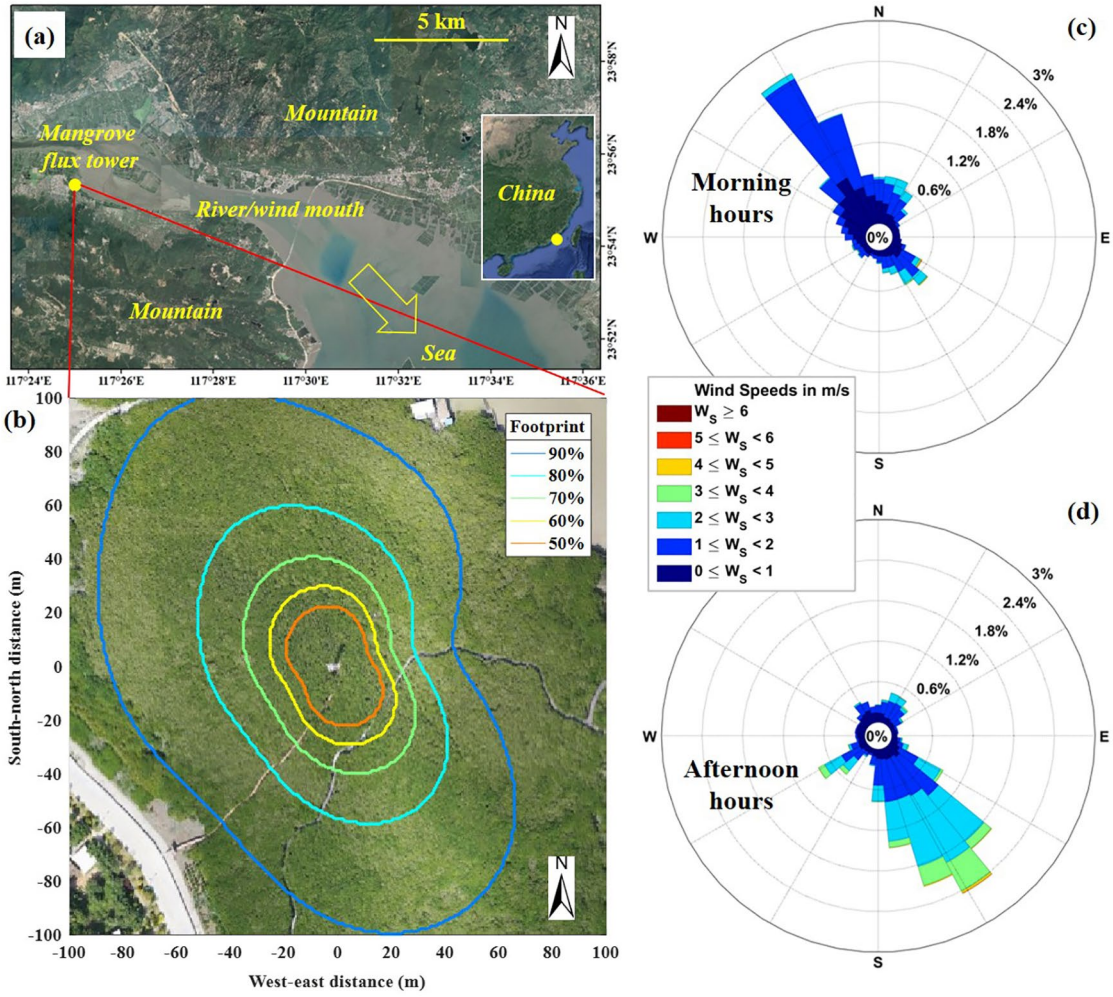

Figure 2. (a) Field site landscape, (b) mangrove flux tower footprint climatology, and (c) and (d) wind rose plots for morning (sunrise-noon) and afternoon (noon-sunset) hours over a 3-year period from July 2016 to June 2019.

3-year data set of EC and ancillary measurements in a subtropical estuarine mangrove wetland. The effects of land breeze on the mangrove NEE are not explicitly examined since the magnitude of land breeze is much smaller than sea breeze for this mangrove wetland. The specific objectives of this study are (1) to examine temporal variations in mangrove NEE across diurnal, daily, and seasonal time scales; (2) to quantify the relative importance of environmental factors in determining mangrove NEE; and (3) to identify the role of land-sea interaction of tidal and sea breeze activity in affecting mangrove NEE.

2. Materials and Methods

2.1. Field Site Description

In-situ time series measurements of EC, meteorological, and tidal data were conducted at a mangrove flux tower (23.9240°N, 117.4147°E; Yunxiao mangrove site of ChinaFLUX) in a subtropical estuarine wetland of southeastern China, which is located inside a river/wind mouth with the open ocean ~30 km to the southeast (Figure 2a). The mangrove forests (mainly comprised of *Kandelia obovata*, *Avicennia marina*, and *Aegiceras corniculatum*) in this wetland are near the northern limit of their habitats in China, having a relatively short and dense canopy structure (varying canopy heights of 3–6 m around the tower averaged at ~4 m, mean tree density of 1.0 individual m^{-2}, and mean leaf area index of 1.7 m^2 m^{-2}) (Zhu, Hou, et al., 2019). The wetland experiences a monsoon climate (most rainfall in spring and summer) and a semidiurnal tidal

cycle (usually inundated twice a day with a mean tidal range of 2.3 m) (Lin, 2001). More detailed information on this field site can be found in Lin (2001) and Zhu, Hou, et al. (2019).

2.2. Eddy Covariance, Meteorological and Tidal Measurements

A variety of in-situ instruments were deployed at the mangrove flux tower to collect time series measurements of EC, meteorological and tidal variables. A 3-year data set of concurrent time series measurements of these variables, from July 2016 to June 2019, were analyzed in this study. An EC system, consisted of a three-axis sonic anemometer (CSAT-3; Campbell Scientific, Inc) and an open path infrared gas analyzer (LI-7500; Li-COR Inc), was mounted on the flux tower (~2 m above the canopy around the tower) to continuously measure NEE between mangrove and the atmosphere. Raw EC data were recorded by a CR3000 data logger (Campbell Scientific, Inc.) at 10 Hz. A typical EC pre-processing procedure, including flux calculations, corrections and quality controls (see Zhu, Song, et al. (2019) for details), was implemented in the EddyPro6.1 software (Li-COR Inc.) to produce half-hourly time series of NEE. Co-spectral analysis confirmed that the EC system was able to capture eddy fluxes of CO_2 across the whole range of frequencies (Figure S1).

Meteorological measurements included wind speed, wind direction, air temperature, VPD, PAR, and rain. Wind speed and direction data were measured using a 010C Wind Speed Sensor (Met One Instruments, Inc) and a 020C Wind Direction Sensor (Met One Instruments, Inc.), respectively. Air temperature and relative humidity were measured using a HMP155A sensor (Vaisala, Helsinki, Finland), and then VPD was derived from air temperature and relative humidity (Murray, 1966). PAR was measured using a PQS1 PAR Quantum sensor (Kipp & Zonen, Delft, Netherlands), and rainfall was measured using a TE525MM Rain Gage (Campbell Scientific, Inc.). Raw 10-minute meteorological measurements, made above the mangrove canopy, were recorded by a CR1000 data logger (Campbell Scientific, Inc.) and processed to half-hourly time series.

Tidal surface water level and salinity were also continuously measured at the flux tower. Tidal surface water level was calculated based on pressure difference from a pair of pressure sensors: one (HOBO U20L-04 Water Level Logger; Onset) was deployed just above sediment surface at the flux tower to measure varying pressures with tidal cycles, and the other (CS106 barometer; Vaisala) was deployed on the flux tower to monitor air pressure. Tidal surface water salinity was estimated from conductivity and temperature measurements using HOBO U24-002-C Conductivity Logger (Onset) deployed just above sediment surface near the flux tower. The salinity was calculated using the Practical Salinity Scale 1978 equations (Lewis & Perkin, 1981) implemented within HOBO Conductivity Assistant Version 2.1 (Onset). The sensor was maintained at each deployment roughly every month during our site visit, including cleaning surface fouling and checking sensor drift with known standard (10 PSU). Raw 10-minute tidal data were consistently converted to half-hourly time series for data analysis.

2.3. Gap Filling of NEE and Other Calculations

The percentage of valid NEE data after the typical EC processing procedure was 47.1% over the 3-year period. For quantifying daily, monthly, and annual carbon exchanges, the missing NEE data were gap-filled based on either look-up table or mean diurnal variation method, following the gap filling algorithm as described in Reichstein et al. (2005). Note that any days or months with valid half-hourly or daily records less than one-third were excluded in the temporal aggregation from half-hourly to daily (23.3% of days were excluded) or from daily to monthly (3 out of 36 months were excluded), and mean values of remaining valid data were used in calculating carbon exchanges at different time scales. To determine the spatial domain of EC signals or the footprint area, the footprint climatology over the 3-year period was calculated from EC instrument setup information and contemporary meteorological measurements, based on the footprint algorithm of Kormann and Meixner (2001). To examine daily sea breeze, half-hourly wind speed/direction data were divided into morning (sunrise-noon) and afternoon (noon-sunset) groups, and afternoon wind speed/direction data were used to represent the status of daily sea breeze (most sea breeze occurs in the afternoon; Figures 2c and 2d). The timing of sunrise and sunset for each day was determined using a PAR threshold of 10 μmol m^{-2} s^{-1}. For a better interpretation, raw wind direction data (0–360° clockwise from the north) was represented by one of the eight directions: north (N), northeast (NE), east (E), southeast (SE), south (S), southwest (SW), west (W), and northwest (NW). The most frequent wind directions in the

morning and afternoon were used for prevailing morning and afternoon wind directions, respectively. To examine the effects of tidal inundation on NEE and other environmental conditions at daily time scale, tidal inundation fraction (0–1) was calculated as temporal fraction of tidal inundated period individually for the whole day, nighttime, and daytime. NEE values were indicated using the meteorological sign convention where downward and upward flux is negative and positive, respectively.

2.4. Statistical Analysis

Spring, summer, autumn, and winter used in the analyses were defined as March–May, June–August, September–November, and December–February, respectively. Rainy days were defined with daily rainfall amount >0 mm over a 24-h period. To examine the impacts of various environmental conditions on the response of daytime half-hourly NEE to PAR, saturating CO_2 assimilation capacity (P_{max}) was used by fitting the Michaelis-Menten rectangular hyperbolic light response equation: $\mathrm{NEE} = -\left(\varepsilon_{max} \times PAR \times P_{max}\right) / \left(\varepsilon_{max} \times PAR + P_{max}\right) + R_{eco}$, where ε_{max} and R_{eco} denote maximum light use efficiency and ecosystem respiration, respectively.

To examine the interaction of various environmental conditions and their direct, indirect, and total effects on NEE, path analysis (or structural equation modeling) was selected to assess the relationships among these different variables at daily time scale (note that, in path analysis, total effect is the sum of direct effect and indirect effect). Exploratory path analysis, one type of multiple regression statistical analysis, is valuable in helping answer many ecological problems emphasizing on understanding the causal relationships with prior knowledge among variables and examining their relative influences and responses (Shipley, 1997; Liu et al., 2019). Six environmental variables were considered in path analyses including PAR, tidal inundation fraction, tidal surface water salinity, sea breeze, air temperature, and VPD. Path analyses were conducted individually for daily, nighttime, and daytime NEE and their concurrent environmental measurements (Figure 3). The logic of structural model of each path analysis was based on prior causal knowledge among NEE and environmental variables. For nighttime NEE, the structural model was established by assuming (Figure 3b): (1) NEE was directly affected by tidal inundation fraction, tidal surface water salinity, and air temperature; (2) tidal inundation fraction directly affected air temperature and then indirectly affected NEE. For daytime and daily NEE, the structural models were established by assuming (Figures 3a and 3c): (1) NEE was directly or indirectly affected by all six environmental variables; (2) PAR directly affected sea breeze and air temperature; (3) tidal inundation fraction directly affected sea breeze, air temperature and VPD; (4) sea breeze directly affected air temperature and VPD; and (5) air temperature directly affected VPD. To ensure a large sample size ($N \geq 200$) required by path analyses (Boomsma & Hoogland, 2001; Kline, 2005), all daily values of the 3-year EC measurements were used in the analyses irrespective of season, since the sample size of any season was insufficient due to data gaps in various variables. In this study, path analysis was implemented by performing a structural equation model with partial least squares using the PLS-SEM Toolbox (Aria, 2019) within MATLAB software (The MathWorks, Inc.).

3. Results

3.1. Temporal Variations in Environmental Conditions and Mangrove NEE

Three-year in-situ wind measurements showed that the coastal wetland had obviously different wind regime between morning and afternoon (Figures 2c–2d and 4a–4b). Northwest or north wind prevailed in the morning (land breeze; accounting for 63.2% of mornings over the 3-year period) with smaller wind speed (mean ± standard deviation: 1.13 ± 0.36 m/s), while southeast or south wind prevailed in the afternoon (sea breeze; accounting for 66.1% of afternoons) with larger wind speed (1.95 ± 0.61 m/s). This contrasting morning/afternoon wind speed and direction (i.e., land/sea breeze switch) was consistent across seasons (Figure S2).

Time series of daily PAR showed strong temporal variations both at short-term (days; regulated by frequent cloudy conditions in coastal area) and long-term (seasons; regulated by varying incoming solar radiation with the Earth's revolution) time scales (Figure 4c). Although the seasonality of daily PAR generally indicated higher (39.6 ± 5.4 mol m^{-2} day^{-1}) and lower (21.9 ± 3.6 mol m^{-2} day^{-1}) values in summer and winter, respectively, daily PAR values of some cloudy summer days were still lower than those of many clear winter

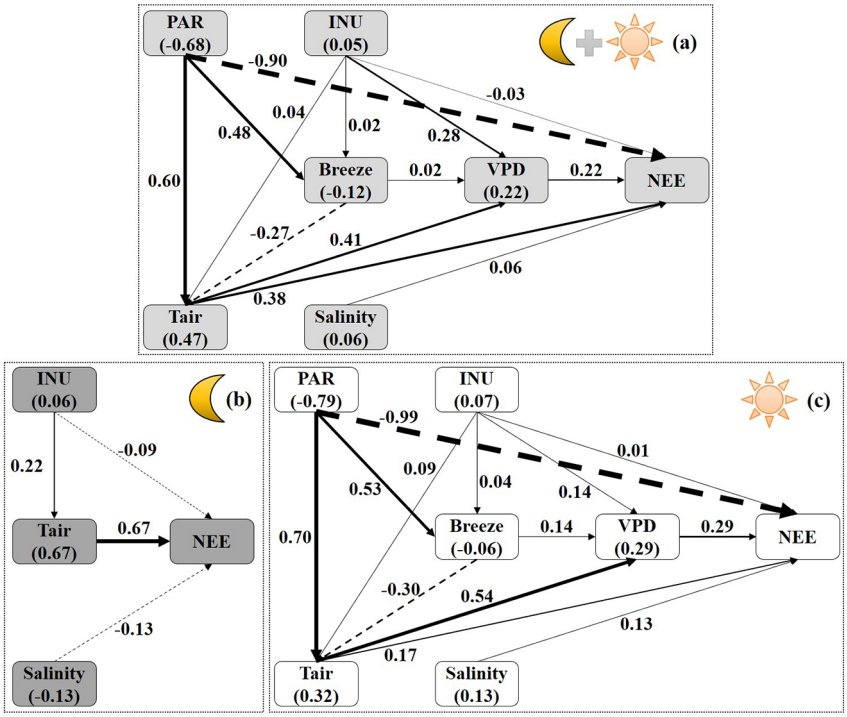

Figure 3. Path diagrams illustrating direct and indirect effects of environmental factors on net ecosystem exchange (NEE) using the 3-year EC measurements. Path analyses were conducted individually for (a) daily, (b) nighttime, and (c) daytime NEE and their concurrent environmental measurements. The magnitude of path coefficient or direct effect along the arrow was proportional to the width of the arrow, and solid and dashed arrows denoted positive and negative direct effects, respectively. The value in parentheses next to each factor is total effect of each factor on NEE, and indirect effect can be calculated as total effect minus direct effect. PAR: cumulative photosynthetically active radiation; INU: tidal inundation fraction; Salinity: mean tidal surface water salinity; Breeze: mean afternoon (noon-sunset) sea breeze; Tair: mean air temperature; VPD: mean vapor pressure deficit.

days. Similar to PAR, time series of daily VPD and air temperature had obvious long-term seasonal trends, but short-term variations of VPD and air temperature were stronger and weaker, respectively, in comparison with PAR (Figures 4c and 4d). Daily VPD varied from 0 to 1.47 kPa and daily air temperature varied from 8.0°C to 32.0°C. The seasonal difference in daily rainfall was also obvious with most (73.3%) of rainfall occurring in spring and summer and the remaining (26.7%) rainfall in autumn and winter (Figure 4d). Rainy days (daily rainfall > 0 mm) accounted for 31.7% over the 3-year period. The temporal change in daily tidal inundation fraction, ranging from 0 (exposed all the time over the day) to 0.27 (inundated 27% of the time) with an average of 0.05, showed a biweekly cycle reflecting the periodic Earth-Moon gravitational interaction. On average, the wetland had larger inundation fraction in autumn (8.9 ± 2.9%) and winter (5.0 ± 1.5%) and smaller inundation fraction in spring (2.8 ± 1.3%) and summer (3.6 ± 1.1%). Daily tidal surface water salinity varied a lot from 0.2 to 18.7 PSU in response to rainfall events and river water inputs (e.g., salinity steeply decreased after rainfall) and seasonally mean value of daily salinity was the lowest (7.60 PSU) and highest (12.17 PSU) in summer and winter, respectively.

Footprint climatology over the 3-year period indicated that 90% of the flux came from an oval-shaped footprint area with a major semi-axis (NW-SE trending) of ~100 m away from the tower, which was fully covered by mangroves (Figure 2b). Time series of daily NEE fluctuated a lot but showed no obvious seasonal pattern (Figure 4f). During the 3-year period, daily NEE ranged from −7.21 to 1.12 g C m^{-2} day^{-1} (averaged at −3.40 g C m^{-2} day^{-1}) with almost all of them negative (i.e., net ecosystem carbon uptake by the wetland). With temporal aggregation, monthly NEE were estimated to −122.6 to −82.2 g C m^{-2} $month^{-1}$ with relatively stronger and weaker carbon sink in spring (−114.7 ± 6.4 g C m^{-2} $month^{-1}$) and autumn (−88.5 ± 5.0 g C m^{-2} $month^{-1}$), respectively. Annual NEE for the full year 2017 and 2018 were estimated to −1255 and −1211 g C m^{-2} $year^{-1}$, respectively.

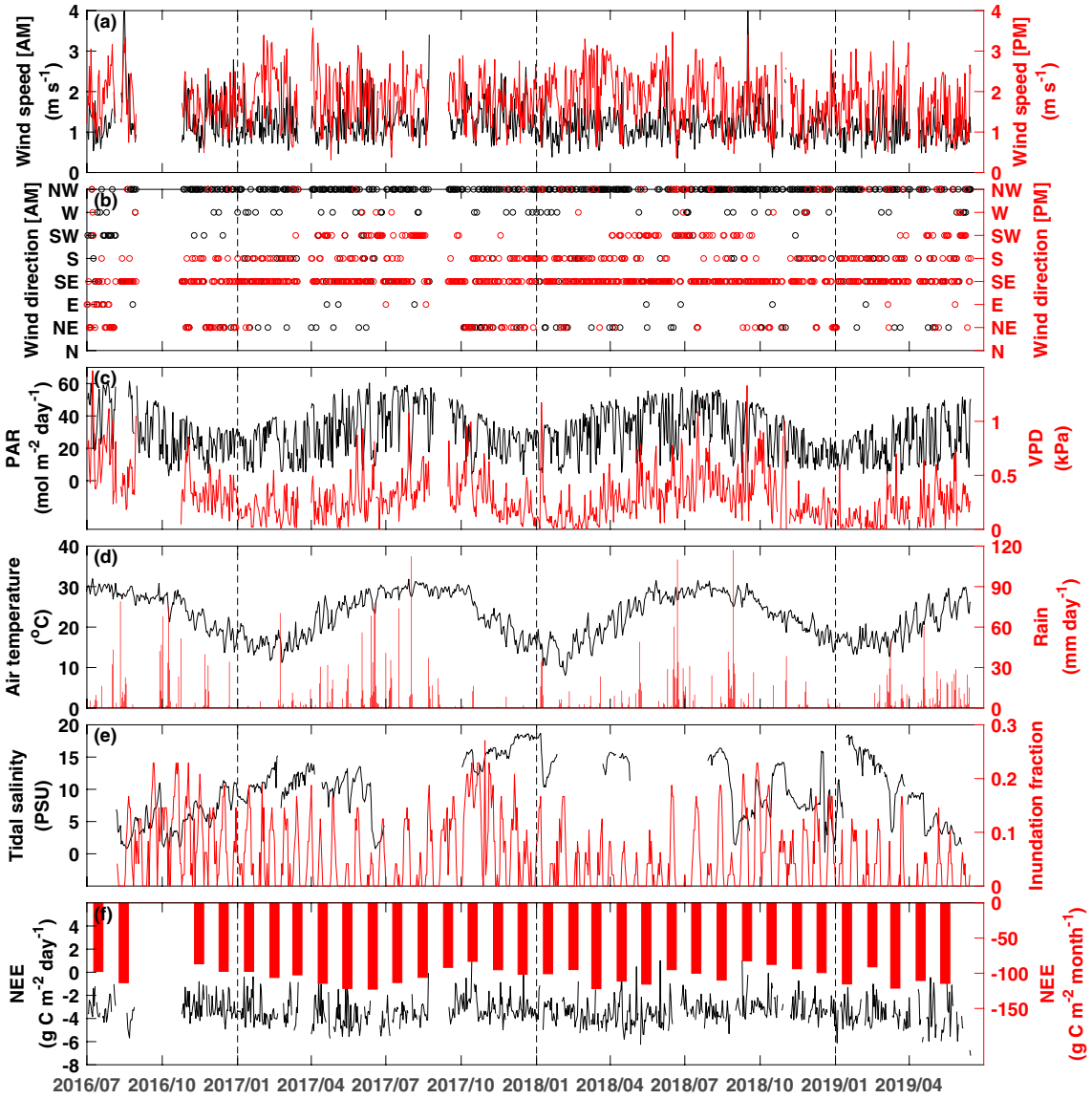

Figure 4. Temporal variations in (a) daily mean morning (sunrise-noon) and afternoon (noon-sunset) wind speed, (b) daily prevailing morning and afternoon wind direction, (c) daily cumulative photosynthetically active radiation (PAR) and daily mean vapor pressure deficit (VPD), (d) daily mean air temperature and daily cumulative rain, (e) daily mean tidal salinity and daily inundation fraction, (f) daily and monthly cumulative gap-filled net ecosystem exchange (NEE). Eight directions were considered for daily prevailing wind directions, and tidal inundation fraction denoted temporal fraction of inundated period. Missing data in daily and monthly (September and October in 2016 and June in 2019) NEE resulted from insufficient valid data in the temporal aggregation. For better reference, seasonal statistical values of each variable are also given in Table S1.

3.2. Impacts of Sea Breeze on Diurnal Variations in Atmospheric Conditions and Mangrove NEE

Daily mean sea breeze speed was found to be significantly ($p < 0.05$) positively related with daily cumulative PAR for each season (Figures 5a–5d). The varying ranges of sea breeze speed among seasons were similar (0.31–3.57 m s^{-1}), but the slopes of PAR-sea breeze linear relationships were larger in spring (0.0336) and winter (0.0337) in comparison with summer (0.0230) and autumn (0.0194). In general, daily mean air temperature was significantly positively related with daily cumulative PAR, and tended to be lower with stronger (higher than the average for the season) sea breeze (Figures 5e–5h). Among seasons, PAR-air temperature relationships were more affected by the magnitude of sea breeze in spring and winter. Similar to PAR-air temperature relationships, daily cumulative PAR and daily mean VPD were positively correlated having lower VPD at stronger sea breeze (Figures 5i–5l).

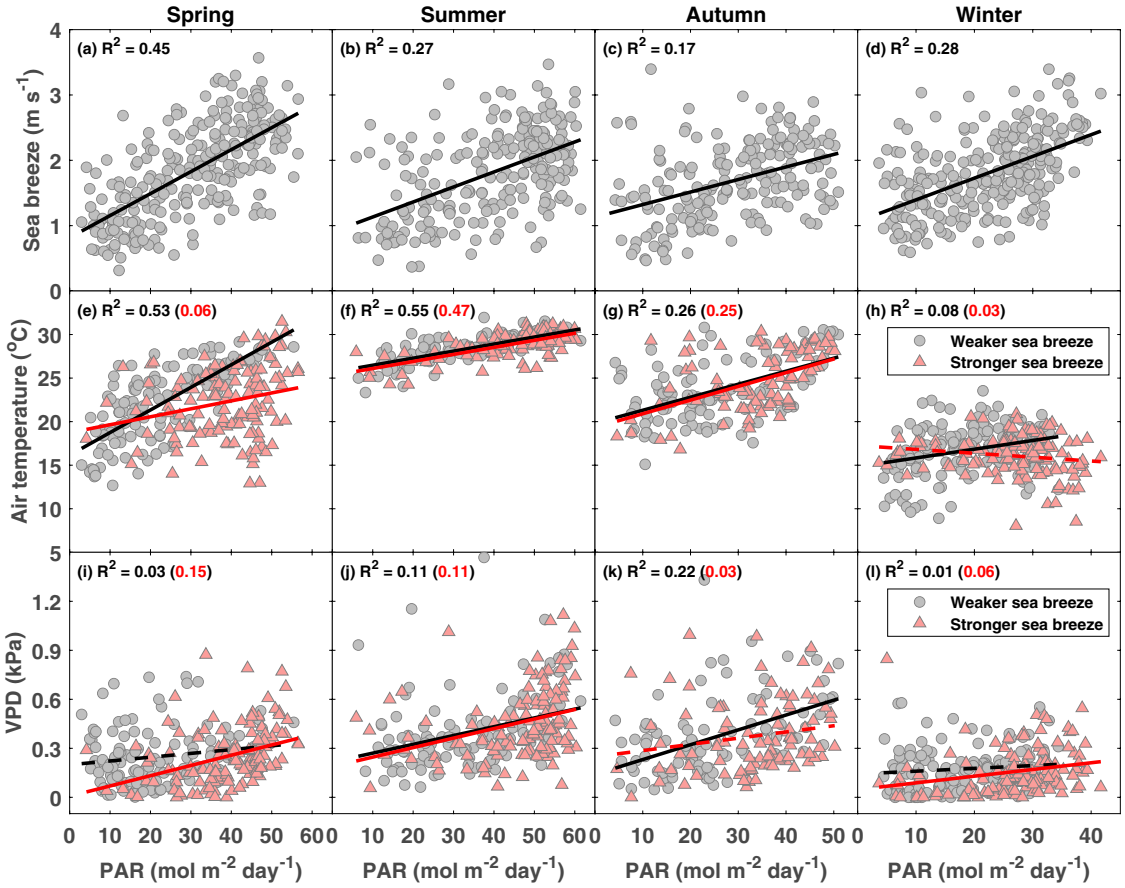

Figure 5. Relationships between daily photosynthetically active radiation (PAR) and (a–d) sea breeze, (e–h) air temperature, and (i–l) vapor pressure deficit (VPD) across seasons, in which PAR-temperature and PAR-VPD scatter plots were grouped by weaker (black) and stronger (red) sea breezes. Mean afternoon (noon-sunset) wind speed within each season (1.85, 1.83, 1.69, and 1.80 m s^{-1} for spring, summer, autumn, and winter, respectively) was used for differentiating days with weaker and stronger sea breezes for that season. A linear regression with R^2 value was shown for each scatter plot (black/red numbers corresponded to weaker/stronger sea breezes) with solid and dashed lines representing statistically significant ($p < 0.05$) and insignificant fitting, respectively.

Mean diurnal variation in half-hourly atmospheric measurements indicated that on average PAR, air temperature/VPD, and sea breeze peaked at noon, ~2 p.m., and ~4 p.m., respectively (Figures 6a–6p). Sea breeze shared a similar diurnal pattern among seasons but the magnitude of peak sea breeze differed among seasons with the strongest (weakest) peak sea breeze in spring (autumn). In line with the positive correlations between daily PAR and sea breeze (Figures 5a–5d), daytime half-hourly PAR with stronger sea breeze was obviously higher than that with weaker sea breeze (Figures 6e–6h). Daytime half-hourly air temperature and VPD were statistically significantly ($p < 0.05$) higher with stronger sea breeze for all seasons except winter, although the difference was relatively smaller in comparison with that in PAR. For each season, daytime half-hourly mangrove NEE was statistically significantly ($p < 0.05$) more negative (i.e., higher carbon sink) with stronger sea breeze (more obvious around noon with the difference up to 3.3 μmol m^{-2} s^{-1}) (Figures 6q–6t).

3.3. Direct and Indirect Effects of Environmental Conditions on Mangrove NEE

Four environmental factors including air temperature, tidal inundation, tidal salinity, and rain were considered in this study to examine the impacts of environmental conditions on half-hourly nighttime mangrove NEE (Figure 7). Half-hourly nighttime NEE was positively related with half-hourly air temperature across seasons. Tidal inundation exerted a negative effect on nighttime CO_2 efflux most of time, and the reduction in mean half-hourly nighttime CO_2 efflux was larger in summer (−0.54 μmol m^{-2} s^{-1}) and autumn (−0.61 μmol m^{-2} s^{-1}) than spring (−0.31 μmol m^{-2} s^{-1}) and winter (−0.43 μmol m^{-2} s^{-1}) (Figures 7a–7d).

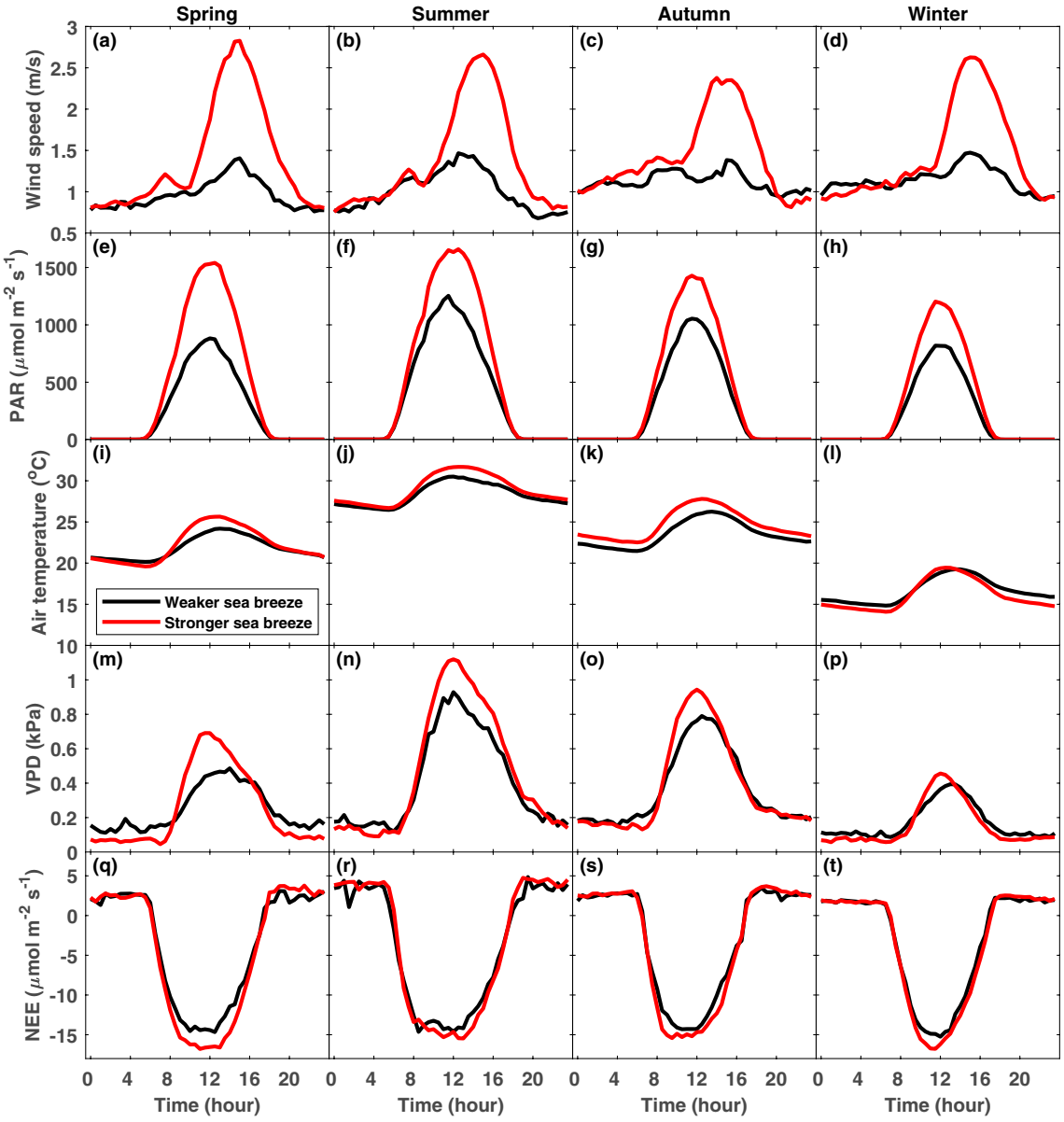

Figure 6. Mean diurnal variations in half-hourly measurements, grouped by weaker and stronger sea breeze across seasons, of (a–d) wind speed, (e–h) photosynthetically active radiation (PAR), (i–l) air temperature, (m–p) vapor pressure deficit (VPD), and (q–t) net ecosystem exchange (NEE). Mean afternoon (noon-sunset) wind speed within each season (1.85, 1.83, 1.69, and 1.80 m s^{-1} for spring, summer, autumn, and winter, respectively) was used for differentiating days with weaker and stronger sea breezes for that season.

The strength of temperature-efflux correlation under inundated condition (correlation coefficient, *r*, varied from 0.35 to 0.87 over seasons; mean $r = 0.64$) was also found to be weaker than that under exposed condition (*r*: 0.62–0.99; mean $r = 0.88$). The effect of tidal surface water salinity on nighttime NEE was slightly positive for spring (0.08 μmol m^{-2} s^{-1}) but negative for other seasons with stronger suppression effects in summer (−0.27 μmol m^{-2} s^{-1}) and autumn (−0.36 μmol m^{-2} s^{-1}) (Figures 7e–7h). In comparison with no rain days, half-hourly nighttime CO_2 efflux was overall slightly suppressed in rainy days (−0.13 μmol m^{-2} s^{-1}, averaged over seasons) with stronger suppression effects in summer (−0.36 μmol m^{-2} s^{-1}) and autumn (−0.18 μmol m^{-2} s^{-1}) (Figures 7i-7l; note that only valid half-hourly NEE data without concurrent rain within that half hour were used here).

In addition to the four environmental controls used for analyzing nighttime mangrove NEE, two more, that is, PAR and VPD, were also considered in examining the response of half-hourly daytime mangrove

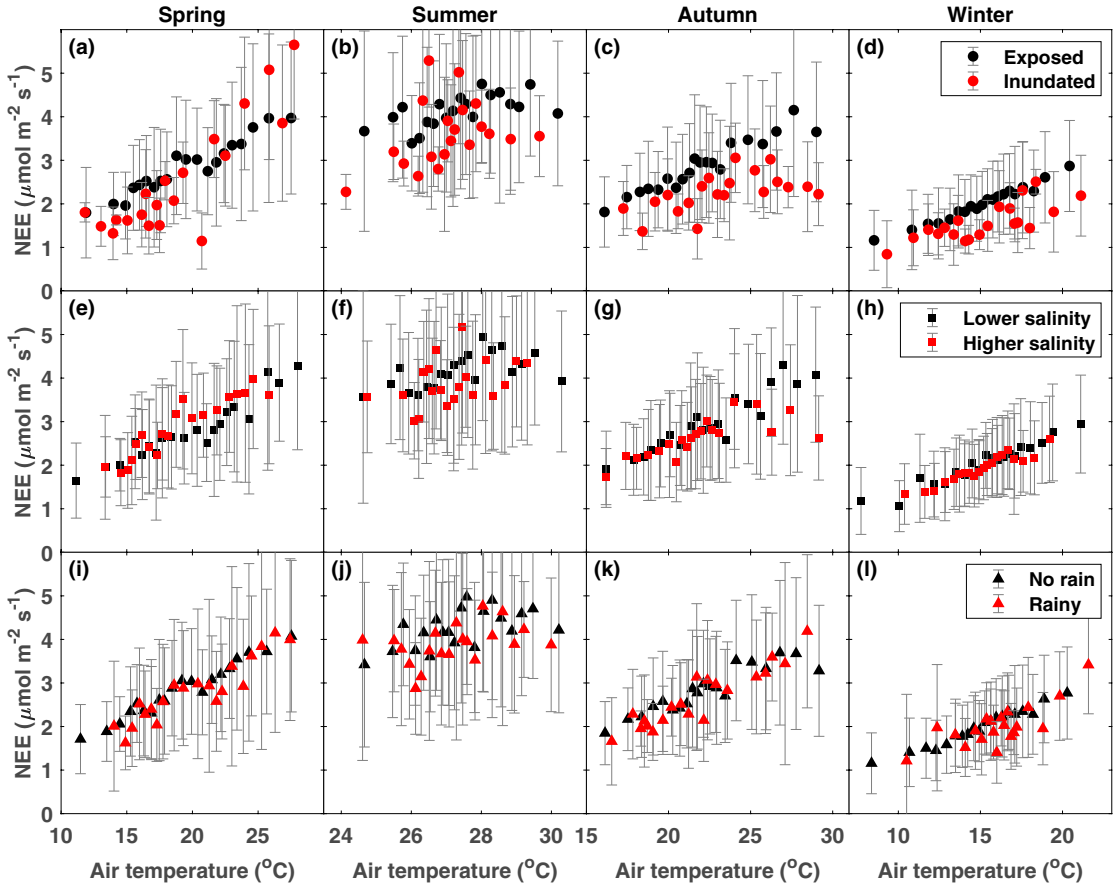

Figure 7. Influences of (a–d) tidal inundation (exposed and inundated), (e–h) tidal salinity (lower and higher salinity), and (i–l) rain conditions (no rain and rainy) on the responses of half-hourly nighttime net ecosystem exchange (NEE) to air temperature across seasons. The NEE data were bin averaged into 20 groups by air temperature, and error bar denoted standard deviation of NEE for each bin. Mean salinity within each season (9.78, 7.60, 8.69, and 12.17 PSU for spring, summer, autumn, and winter, respectively) was used for differentiating days with lower and higher salinity for that season.

NEE to varying environmental conditions (Figure 8). The variation of half-hourly daytime NEE with PAR followed typical light-response curves for all seasons, where CO_2 assimilation rate increased nonlinearly with PAR and saturated at ~15 μmol m^{-2} s^{-1} with PAR >~1000 μmol m^{-2} s^{-1}. The impacts of tidal inundation and salinity on the light-response curve were not obvious (Figures 8a–8h), while the impacts of rain, air temperature, and VPD on the light-response curves can be identified (Figure 8i–8t). In comparison with no rain days, saturating CO_2 assimilation capacity (P_{max}; positive value) fitted from the light-response curve was consistently stronger at rainy days across seasons (the change in P_{max}: 1.07–2.90 μmol m^{-2} s^{-1}). For air temperature, P_{max} at higher temperature was stronger in spring (1.48 μmol m^{-2} s^{-1}) and winter (2.74 μmol m^{-2} s^{-1}) but weaker in summer (−7.08 μmol m^{-2} s^{-1}) and autumn (−5.94 μmol m^{-2} s^{-1}). For VPD, P_{max} was consistently weaker at higher VPD across seasons (−2.27 to −6.34 μmol m^{-2} s^{-1}).

At daily time scale, the mangrove NEE was directly and indirectly affected by a variety of environmental variables. The importance of direct, indirect, and total effects of each environmental variable on nighttime, daytime, and daily NEE were quantified based on path analyses using EC measurements over the 3-year period (Figure 3). Nighttime NEE was dominantly affected by air temperature with a strong positive direct effect of 0.67, while tidal salinity had a negative direct effect (−0.13) on nighttime NEE (Figure 3b). Tidal inundation exerted a negative direct effect (−0.09) on nighttime NEE but a positive indirect effect (0.15; total effect minus direct effect) on nighttime NEE via adjusting air/soil temperature, resulting in a positive total effect of 0.06. For daytime NEE, the importance of total effect generally decreased in the order of PAR (−0.79), air temperature (0.32), VPD (0.29), tidal salinity (0.13), tidal inundation (0.07) and sea breeze (−0.06) (Figure 3c). Both of direct (−0.99) and indirect effects (0.20) of PAR on NEE were the

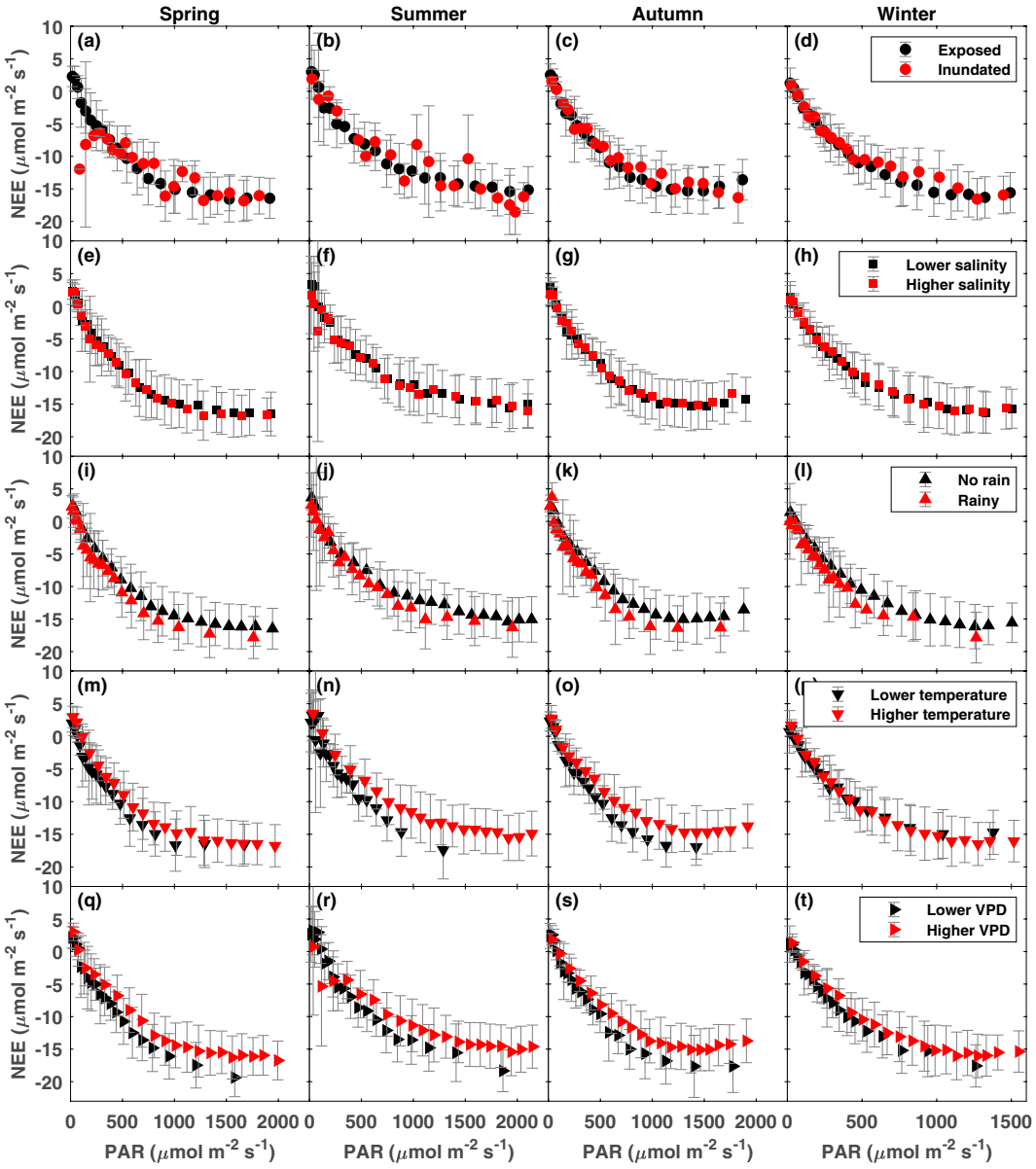

Figure 8. Influences of (a–d) tidal inundation (exposed and inundated), (e–h) tidal salinity (lower and higher), (i–l) rain conditions (no rain and rainy), (m–p) air temperature (lower and higher) and (q–t) vapor pressure deficit (VPD, lower and higher) on the responses of half-hourly daytime net ecosystem exchange (NEE) to photosynthetically active radiation (PAR) across seasons. The NEE data were bin averaged into 20 groups by PAR, and error bar denoted standard deviation of NEE for each bin. Mean salinity/temperature/VPD within each season (salinity: 9.78, 7.60, 8.69, and 12.17 PSU; temperature: 22.06°C, 28°C.65°C, 24.85°C, and 16.41°C; mean VPD: 0.25, 0.43, 0.37, and 0.16 kPa; in the order of spring, summer, autumn, and winter) was used for differentiating days with lower and higher values for that season.

strongest among these variables. Air temperature had moderate direct (0.17) and indirect (0.15) effects on NEE. VPD (0.29) and tidal salinity (0.13) had only direct effect on NEE, while sea breeze had only indirect effect (−0.06) on NEE. Tidal inundation exerted both direct (0.01) and indirect (0.06) effects on NEE, but the importance of them were weak. When both nighttime and daytime NEE was combined into daily (nighttime + daytime) NEE, the order of the importance of total effect did not differ from that of daytime NEE, although the relative magnitude of direct/indirect effect changed (e.g., stronger direct effect of air temperature on daily NEE than daytime NEE) (Figure 3a).

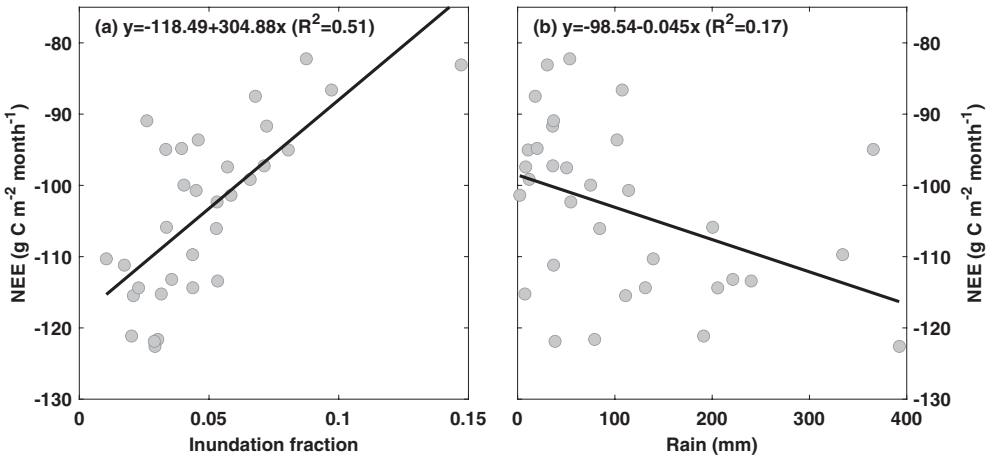

Figure 9. Monthly accumulated net ecosystem exchange (NEE) as a function of (a) monthly mean tidal inundation fraction and (b) monthly accumulated rain. Linear regressions fitted for the two relationships were both statistically significant ($p < 0.05$).

At monthly time scale, correlation analyses were further conducted to examine potential relationship between mangrove NEE and various environmental variables (PAR, air temperature, tidal inundation fraction, tidal salinity, VPD, sea breeze, and rain). Among these environmental variables, only tidal inundation fraction and rain were statistically correlated ($p < 0.05$) with NEE (Figure 9). Monthly tidal inundation fraction was statistically positively correlated with monthly NEE showing less negative NEE at larger inundation fraction. Monthly rain was statistically negatively correlated with monthly NEE showing more negative NEE at more rainfall.

4. Discussion

4.1. Relief of Sea Breeze to Meteorological Stresses on Mangrove NEE

In addition to the difference in PAR among seasons, the seasonal contrast in the strength of sea breeze and its cooling and wetting effects on coastal meteorological conditions might also be attributed to the difference in tidal inundation among seasons (Figure 4e), since strong tidal activity might strengthen sea breeze through the dynamic effect of tidal currents and through the thermal effect of flooding/drying mudflats (Fischereit et al., 2016): tides influenced sea breeze by changing surface friction, roughness length, and area fraction of flooding/drying mudflats over the intertidal area, as well as the extent of in-land penetration of sea breeze front and its distance from the EC flux tower. Although sea breeze and PAR were significantly positively correlated (Figures 5a–5d), the relative magnitude of sea breeze was not consistent with that of PAR across seasons (Figures 6a–6h). For instance, the season with the strongest sea breeze (spring) did not correspond to that with the largest PAR (summer), and the season with the weakest sea breeze (autumn) did not correspond to that with the smallest PAR (winter). This inconsistency suggested that factors other than PAR (possibly tidal activity) could affect the strength of sea breeze.

The fact that air temperature and VPD were generally higher under stronger sea breeze condition (Figures 6i–6p) was not in conflict with previously confirmed negative effect of sea breeze on air temperature and VPD. In fact, diurnal variations in air temperature and VPD were overwhelmingly dominated by diurnal variation in PAR with down-regulation by sea breeze. Although higher carbon sink (i.e., more negative NEE) was apparently associated with stronger sea breeze across seasons (Figures 6q–6t), this apparent effect cannot simply be considered as the contribution from sea breeze since many other environmental factors were also involved in affecting mangrove NEE. Diurnal variation in half-hourly measurements did not synchronize each other with PAR and NEE peaking around noon, followed by air temperature/VPD and sea breeze peaking about two and four hours later, respectively. Therefore, the interaction among these asynchronous meteorological factors and their influences on half-hourly NEE could change over the course of the day. For example, diurnal course of half-hourly VPD was asymmetric with faster decline in VPD beyond

the time of peaking value, due to the wetting effect of sea breeze peaking late in the afternoon (Figures 6a–6d vs. Figures 6m–6p). Given that the significant suppression effect of increasing VPD on surface conductance has been well recognized across ecosystems (Novick et al., 2016; Oren et al., 1999), sea breeze-induced lower VPD can relieve atmospheric stresses on mangrove photosynthesis leading to an enhanced carbon uptake. Also, midday depression of plant photosynthesis usually occurred due to stomatal closure at high VPD (Xu & Shen, 1996), and it might be more severe for mangrove forests since they experienced additional tidal stresses (inundation and salinity) in addition to atmospheric stresses (Alongi, 2009). Regular arrivals of sea breeze in the afternoon can lead to weaker midday depression of photosynthesis in mangrove forests.

4.2. Environmental Controls on Half-Hourly Mangrove NEE

The magnitude of nighttime NEE (mostly ranging from 1 to 5 μmol m^{-2} s^{-1}) in this mangrove wetland was comparable with the measurements in previous mangrove EC studies (Barr et al., 2010; Leopold et al., 2016). Consistent with these studies, nighttime CO_2 efflux was found to be much lower than daytime CO_2 assimilation. The dominant positive effect of air temperature on nighttime NEE was confirmed at half-hourly time scale (Figure 7), since both autotrophic and heterotrophic respiration are highly temperature-dependent. With low nighttime NEE, the relationship between half-hourly nighttime NEE and air temperature appeared to be linear instead of exponential as commonly thought, which was consistent with other studies having similar magnitude of nighttime NEE (Barr et al., 2010) but different from those having larger nighttime CO_2 efflux (Liu & Lai, 2019). The lower half-hourly nighttime NEE with tidal inundation in this mangrove wetland confirmed the suppression effect of tidal inundation on CO_2 efflux at sub-daily time scale, which was relatively well understood by the community (Barr et al., 2010; Leopold et al., 2016; Q. Li et al., 2014; Liu & Lai, 2019). The weaker temperature-efflux correlations with tidal inundation across seasons reflected the tidal disturbances on CO_2 efflux, presumably due to the combination of anoxia-induced reduction in ecosystem respiration and physical barrier of gas diffusion (Barr et al., 2010; Q. Li et al., 2014). Although high salinity can influence both autotropic and heterotrophic respiration in mangrove wetlands (Robertson & Alongi, 2016; Takemura et al., 2000), inhibitory effects of salinity might not be observed at a moderate level of <20 PSU (N. Li et al., 2008; Ye et al., 2010). Tidal salinity in this mangrove wetland fluctuated with time within 0–20 PSU (Figure 4e), which could explain why there was no strong positive or negative effect of tidal salinity on nighttime NEE (Figures 7e–7h and S3). In comparison with tidal inundation, rain exerted a similar but weaker suppression effect on nighttime NEE (Figures 7i–7l vs. Figures 7a–7d). It is possible that heavy rainfall resulted in surface inundation but the extent was much less than tidal inundation. When tidal inundation, salinity, and rainy conditions were taken together, the response of nighttime NEE to air temperature at half-hourly time scale were always more down-regulated by these three factors in summer and autumn in comparison with spring and winter, which implied that NEE in hot seasons was less temperature-dominated with larger impacts from other factors.

Although the light-response curves showed consistently stronger saturating CO_2 assimilation capacity (P_{max}) at rainy days, a higher P_{max} in a rainy day did not necessarily lead to a larger daytime carbon assimilation since rainy days usually came with much lower PAR (Figures 8i–8l). The contrasting impacts of lower/higher temperature on the light-response curves between hot and cold seasons suggested that both high temperature in hot seasons and low temperature in cold seasons could limit mangrove carbon assimilation. The effect of VPD on the light response curve was more obvious and consistent across seasons in comparison with other factors (as indicated by the largest difference in P_{max} between lower and higher VPD), which highlighted the important role of VPD in affecting daytime carbon uptake. The stronger suppression effects of high temperature and VPD in summer and autumn implied that the sensitivity of light-response curves to temperature and VPD varied across seasons.

4.3. Environmental Controls on Daily Mangrove NEE

The dominant role of air temperature on nighttime NEE at daily time scale was further confirmed by path analysis (Figure 3b). In contrast with the negative effect of tidal inundation at half-hourly time scale, tidal inundation exerted a positive total effect on nighttime NEE at daily time scale with negative direct effect overweighed by positive indirect effect. This finding suggested that, at daily time scale, the positive effect of tidal inundation on nighttime NEE due to enhanced air temperature (Figure S4) was more important

than the negative effect due to oxygen/diffusion limitation. The "heat capacitor" role of tidal floodwaters found in this mangrove ecosystem was consistent with previous energy budget measurements in coastal ecosystems (McGowan et al., 2010; Moffett et al., 2010). This indirect positive effect of tidal inundation also applied to half-hourly nighttime NEE, but it might not be immediately observed due to the time-lag in heat transfer from warmer tidal floodwaters at nighttime (Barr, Fuentes, et al., 2013). For daytime NEE, it was not intuitive to interpret indirect effects of environmental factors since they formed a complex interactive network (Figure 3c), but it can be concluded that indirect effects were not negligible with the magnitude comparable to or even larger than direct effects in some cases. For example, direct effect of PAR on daytime NEE was partially (20%) offset by its indirect effect via five paths (PAR → Tair → NEE, PAR → Tair → VPD → NEE, PAR → breeze → VPD → NEE, PAR → breeze → Tair → NEE, PAR → breeze → Tair → VPD → NEE), indicating that increasing PAR also had adverse effects on mangrove carbon uptake. For another example, the indirect effect of air temperature on daytime NEE via VPD roughly equaled to its direct effect, suggesting that both indirect and direct effects of air temperature played equally important roles in suppressing mangrove carbon uptake.

4.4. Environmental Controls on Monthly Mangrove NEE

The seasonal variation in monthly NEE in this wetland was weak but with stronger carbon sink capacity in spring (Figure 4f), which was consistent with many previous studies (Barr et al., 2010; Leopold et al., 2016; Liu & Lai, 2019). Correlation analyses highlighted the important roles of tidal inundation fraction and rain in affecting mangrove NEE at monthly time scale (Figure 9). The strong positive correlation between monthly NEE and tidal inundation fraction suggested that tidal inundation fraction could suppress mangrove carbon sink (less negative NEE) at monthly time scale (Figure 9a). The difference in the impacts of tidal inundation fraction on mangrove NEE among half-hourly (negative; Figures 7a–7d), daily (positive; Figure 3), and monthly (positive; Figure 9a) time scales suggested that the influence of tidal inundation fraction on NEE shifted from a negative effect at shorter time scale (half-hourly) to a positive effect at longer time scales (daily and monthly). This finding seemed counterintuitive, but it could result from the change in relative contribution of direct and indirect effects of tidal activity across time scales. The negative correlation between NEE and rain (Figure 9b) was relatively weaker but still statistically significant ($p < 0.05$), which implied that in this wetland more rainfall could stimulate mangrove carbon uptake (more negative NEE) to a certain extent. This finding was consistent with previous reports showing positive link between annual rain and mangrove carbon stocks or sinks (Leopold et al., 2016; Sanders et al., 2016; Simard et al., 2019), but different from (Liu & Lai, 2019) showing a negative impact of monthly rain on carbon sink in another subtropical mangrove wetland. In fact, across mangrove sites with different rainfall gradients, both of positive and negative impacts are possible since rain can exert both direct and indirect effects. Moderate amount of rain could relieve the salinity stress of mangrove forests (tidal salinity was statistically negatively correlated with rain at monthly time scale in this wetland; Figure S5), but too much rain usually accompanies with a large reduction in PAR leading to a lowered carbon uptake. The annual rain in this mangrove wetland (averaged at ~1200 mm for year 2017 and 2018) is much lower than that (~1750 mm) of (Liu & Lai, 2019), which could explain the contrasting results on the impact of rain on monthly mangrove carbon uptake.

4.5. Limitations and Uncertainties

The analyses of mangrove NEE and its environmental controls in this study suffered from several limitations and uncertainties. First, tide-related horizontal export of DIC from soil respiration (Alongi, 2014) could not be captured by EC measurements and thus EC-induced carbon uptake might be overestimated without considering this export effect. Second, due to much shorter inundation (~5% of the time) versus exposed (~95%) period, there could be a larger uncertainty in assessing the impacts of tidal inundation on mangrove NEE with smaller sample size. Further assessment with longer-term measurements in the future are needed to reduce this uncertainty. Third, surface water salinity is not necessarily equivalent to subsurface porewater salinity, which is usually higher and presumably exerts a stronger effect on mangrove productivity than surface water salinity. Thus, further analyses on the salinity effect on mangrove NEE should be conducted in future when long-term continuous measurement of subsurface porewater salinity is available. Fourthly, the spatial heterogeneity of the three mangrove species within the EC footprint also

affected mangrove NEE and subsequent analyses since the change in wind speed/direction directly influenced the EC flux footprint (Figure S6), but unfortunately this cannot be explicitly assessed in this study due to the lack of species-dependent information on carbon exchange. Despite of varying footprint area and the spatial heterogeneity within the footprint, our previous airborne-LiDAR field campaign confirmed that this mangrove forest was relatively homogeneous in terms of canopy structure and understory topography within the EC footprint (Zhu, Hou, et al., 2019), and thus this footprint issue could exert a relatively small effect on mangrove NEE. Fifthly, although path analyses used in this study helped quantify the relative strength of correlations between mangrove NEE and various environmental factors, it should keep in mind that correlation should never be confused with causation and that path coefficients could vary with different combination/hypothesis of input variables. Considering the potential of temporal autocorrelation that could produce spurious statistical significance (Dodds et al., 2013), the results of path analyses should be also taken with caution. Further investigations on the uncertainty in path analyses and more prior knowledge are needed to confirm the causation. Sixthly, although sea breeze-induced relief to atmospheric demand has been confirmed in this study to explain enhanced carbon uptake with strong sea breeze in the afternoon, future studies with direct evidence on the change in stomatal conductance are needed to acquire deeper mechanistic understanding on how sea breeze explicitly affect stomatal conductance and subsequent carbon fluxes. Lastly, the interactive effects of environmental factors were not fully considered in this study. For example, we individually analyzed the effect of tidal inundation, surface water salinity, and rainfall, but in fact these factors were closely correlated: for no rain days the variations in tidal inundation and surface water salinity were mainly determined by tidal seawater and river freshwater inputs, while for rainy days the variations were obviously affected by the amount of rainfall, in particular for surface water salinity. This limitation should be also kept in mind and require further investigation.

5. Conclusions

In summary, continuous EC and auxiliary measurements from July 2016 to June 2019 were explored to characterize temporal variations in NEE and environmental controls in a subtropical mangrove of southeastern China. Over the three-year period, this mangrove acted a consistent carbon sink and showed weak seasonality in NEE with a stronger sink in spring. Environmental controls on mangrove NEE varied across half-hourly, daily, and monthly time scales. Indirect effects of some environmental factors on NEE might play as important roles as direct effects: (1) periodic tidal inundation exerted both direct and indirect effects, but their relative importance changed across time scales; (2) cooling and wetting effects from regular sea breeze relieved atmospheric temperature/moisture stresses at afternoon, acting as an important indirect impact of sea breeze to promote carbon uptake. This study confirms the importance of previously neglected indirect effects of land-sea interaction of tidal and sea breeze activity on mangrove NEE. Given that tide and sea breeze is regular phenomenon throughout the year in tropical and subtropical coastal regions, their impacts on carbon cycling of mangrove ecosystem (or other coastal ecosystems) should be common worldwide. Due to the strong negative link between mangrove NEE and air temperature/tidal inundation, mangrove wetlands could become a weaker blue carbon sink in response to global warming and sea level rise in the future. Future changes in the amount or pattern of rainfall could also influence mangrove carbon exchange. Both direct and indirect effects of environmental factors including tidal and sea breeze activity should be explicitly considered in future studies in examining temporal variations in mangrove carbon exchange and their environmental controls across time scales.

Data Availability Statement

The data necessary to reproduce key findings in this paper can be accessed at http://doi.org/10.5281/zenodo.4382202.

Acknowledgments
The authors thank Yuwen Hou, Kangming Chen, Chenyang Sun, Chenjuan Zheng and Guanmin Huang for their help in the field work. The authors thank the Zhangjiang Estuary Mangrove National Nature Reserve for its long-term support to our ecological research program. The authors also thank ChinaFLUX and the U.S.-China Carbon Consortium (USCCC) for helpful discussions and exchange of ideas. This study was supported by the National Key Research and Development Program of China (2017YFC0506102), the National Natural Science Foundation of China (31600368), the Natural Science Foundation of Fujian Province, China (2017J01069, 2020J01112079), the Youth Innovation Foundation of Xiamen, China (3502Z20206038), the Fundamental Research Funds for the Central Universities of China (20720180118, 20720190104), the Key Laboratory of the Coastal and Wetland Ecosystems (WELRI201601) and the State Key Laboratory of Marine Environmental Science (MELRI1603).

References

Alongi, D. M. (2009). *The energetics of mangrove forests*. Springer Netherlands.
Alongi, D. M. (2012). Carbon sequestration in mangrove forests. *Carbon Management*, *3*, 313–322.
Alongi, D. M. (2014). Carbon cycling and storage in mangrove forests. *Annual Review of Marine Science*, *6*, 195–219.

Aria, M. (2019). *PLS-SEM Toolbox*. MATLAB Central File Exchange Retrieved December 15, 2019. Retrieved from https://www.mathworks.com/matlabcentral/fileexchange/54147-pls-sem-toolbox

Baldocchi, D., Falge, E., Gu, L., Olson, R., Hollinger, D., Running, S., et al. (2001). FLUXNET: A new tool to study the temporal and spatial variability of ecosystem–scale carbon dioxide, water vapor, and energy flux densities. *Bulletin of the American Meteorological Society*, *82*, 2415–2434.

Barr, J. G., Engel, V., Fuentes, J. D., Fuller, D. O., & Kwon, H. (2013). Modeling light use efficiency in a subtropical mangrove forest equipped with CO_2 eddy covariance. *Biogeosciences*, *10*, 2145–2158.

Barr, J. G., Engel, V., Fuentes, J. D., Zieman, J. C., O'halloran, T. L., Smith, T. J., & Anderson, G. H. (2010). Controls on mangrove forest-atmosphere carbon dioxide exchanges in western Everglades National Park. *Journal of Geophysical Research*, *115*, G02020. https://doi.org/10.1029/2009JG001186

Barr, J. G., Fuentes, J. D., DeLonge, M. S., O'Halloran, T. L., Barr, D., & Zieman, J. C. (2013). Summertime influences of tidal energy advection on the surface energy balance in a mangrove forest. *Biogeosciences*, *10*, 501–511.

Boomsma, A., & Hoogland, J. J. (2001). The robustness of LISREL modeling revisited. In *Structural equation models: Present and future. A Festschrift in honor of Karl Jöreskog* (pp. 139–168) Scientific Software International.

Chen, L., Wang, W., Li, Q. Q., Zhang, Y., Yang, S., Osland, M. J., et al. (2017). Mangrove species' responses to winter air temperature extremes in China. *Ecosphere*, *8*, e01865.

Chu, H., Baldocchi, D. D., John, R., Wolf, S., & Reichstein, M. (2017). Fluxes all of the time? A primer on the temporal representativeness of FLUXNET. *Journal of Geophysical Research: Biogeosciences*, *122*, 289–307. https://doi.org/10.1002/2016JG003576

Crase, B., Vesk, P. A., Liedloff, A., & Wintle, B. A. (2015). Modelling both dominance and species distribution provides a more complete picture of changes to mangrove ecosystems under climate change. *Global Change Biology*, *21*, 3005–3020.

Cui, X., Liang, J., Lu, W., Chen, H., Liu, F., Lin, G., et al. (2018). Stronger ecosystem carbon sequestration potential of mangrove wetlands with respect to terrestrial forests in subtropical China. *Agricultural and Forest Meteorology*, *249*, 71–80.

Dodds, W. K., Veach, A. M., Ruffing, C. M., Larson, D. M., Fischer, J. L., & Costigan, K. H. (2013). Abiotic controls and temporal variability of river metabolism: Multiyear analyses of Mississippi and Chattahoochee River data. *Freshwater Science*, *32*, 1073–1087.

Fischereit, J., Schlünzen, K. H., Gierisch, A. M., Grawe, D., & Petrik, R. (2016). Modelling tidal influence on sea breezes with models of different complexity. *Meteorologische Zeitschrift*, *25*(4), 343–355.

Friess, D. A., Rogers, K., Lovelock, C. E., Krauss, K. W., Hamilton, S. E., Lee, S. Y., et al. (2019). The state of the World's mangrove forests: Past, present, and future. *Annual Review of Environment and Resources*, *44*, 89–115.

Howard, J., Hoyt, S., Isensee, K., Telszewski, M., & Pidgeon, E. (2014). *Coastal blue carbon: Methods for assessing carbon stocks and emissions factors in mangroves, tidal salt marshes, and seagrasses*. Conservation International, Intergovernmental Oceanographic Commission of UNESCO, International Union for Conservation of Nature.

Howard, J., Sutton-Grier, A., Herr, D., Kleypas, J., Landis, E., Mcleod, E., et al. (2017). Clarifying the role of coastal and marine systems in climate mitigation. *Frontiers in Ecology and the Environment*, *15*, 42–50.

Huang, Y., Guo, H., Chen, X., Chen, Z., Van Der Tol, C., Zhou, Y., & Tang, J. (2019). Meteorological controls on evapotranspiration over a coastal salt marsh ecosystem under tidal influence. *Agricultural and Forest Meteorology*, *279*, 107755.

Hursh, A., Ballantyne, A., Cooper, L., Maneta, M., Kimball, J., & Watts, J. (2017). The sensitivity of soil respiration to soil temperature, moisture, and carbon supply at the global scale. *Global Change Biology*, *23*, 2090–2103.

Jiang, S., Lu, H., Liu, J., Lin, Y., Dai, M., & Yan, C. (2018). Influence of seasonal variation and anthropogenic activity on phosphorus cycling and retention in mangrove sediments: A case study in China. *Estuarine, Coastal and Shelf Science*, *202*, 134–144.

Kline, R. B. (2005). *Principles and practice of structural equation modeling*. Guilford.

Kormann, R., & Meixner, F. X. (2001). An analytical footprint model for non-neutral stratification. *Boundary-Layer Meteorology*, *99*, 207–224.

Leopold, A., Marchand, C., Renchon, A., Deborde, J., Quiniou, T., & Allenbach, M. (2016). Net ecosystem CO_2 exchange in the "Coeur de Voh" mangrove, New Caledonia: Effects of water stress on mangrove productivity in a semi-arid climate. *Agricultural and Forest Meteorology*, *223*, 217–232.

Lewis, E. L., & Perkin, R. G. (1981). The practical salinity scale 1978: Conversion of existing data. *Deep Sea Research Part A. Oceanographic Research Papers*, *28*, 307–328.

Li, N., Chen, S., Zhou, X., Li, C., Shao, J., Wang, R., et al. (2008). Effect of NaCl on photosynthesis, salt accumulation and ion compartmentation in two mangrove species, *Kandelia candel* and *Bruguiera gymnorhiza*. *Aquatic Botany*, *88*, 303–310.

Li, Q., Lu, W., Chen, H., Luo, Y., & Lin, G. (2014). Differential responses of net ecosystem exchange of carbon dioxide to light and temperature between spring and neap tides in subtropical mangrove forests. *Science World Journal*, *2014*. 943697. https://doi.org/10.1155/2014/943697

Lin, P. (2001). *The comprehensive report of science investigation on the natural reserve of mangrove wetland of Zhangjiang Estuary in Fujian*. Xiamen University Press.

Liu, J., & Lai, D. Y. (2019). Subtropical mangrove wetland is a stronger carbon dioxide sink in the dry than wet seasons. *Agricultural and Forest Meteorology*, *278*, 107644.

Malone, S. L., Barr, J., Fuentes, J. D., Oberbauer, S. F., Staudhammer, C. L., Gaiser, E. E., & Starr, G. (2016). Sensitivity to low-temperature events: Implications for CO_2 dynamics in subtropical coastal ecosystems. *Wetlands*, *36*, 957–967.

McGowan, H. A., Sturman, A. P., MacKellar, M. C., Wiebe, A. H., & Neil, D. T. (2010). Measurements of the local energy balance over a coral reef flat, Heron Island, southern Great Barrier Reef, Australia. *Journal of Geophysical Research*, *115*(D19), D19124. https://doi.org/10.1029/2010JD014218

Mcleod, E., Chmura, G. L., Bouillon, S., Salm, R., Björk, M., Duarte, C. M., et al. (2011). A blueprint for blue carbon: Toward an improved understanding of the role of vegetated coastal habitats in sequestering CO_2. *Frontiers in Ecology and the Environment*, *9*, 552–560.

Miller, S., Keim, B., Talbot, R., & Mao, H. (2003). Sea breeze: Structure, forecasting, and impacts. *Reviews of Geophysics*, *41*, 1011. https://doi.org/10.1029/2003RG000124

Moffett, K. B., Wolf, A., Berry, J. A., & Gorelick, S. M. (2010). Salt marsh-atmosphere exchange of energy, water vapor, and carbon dioxide: Effects of tidal flooding and biophysical controls. *Water Resources Research*, *46*, W10525. https://doi.org/10.1029/2009WR009041

Murray, F. W. (1966). *On the computation of saturation vapor pressure*. RAND CORPORATION SANTA MONICA CALIFORNIA.

Nellemann, C., & Corcoran, E. (2009). *Blue carbon: The role of healthy oceans in binding carbon: A rapid response assessment*. UNEP/Earthprint.

Novick, K. A., Ficklin, D. L., Stoy, P. C., Williams, C. A., Bohrer, G., Oishi, A. C., et al. (2016). The increasing importance of atmospheric demand for ecosystem water and carbon fluxes. *Nature Climate Change*, *6*, 1023–1027.

Oren, R., Sperry, J., Katul, G., Pataki, D., Ewers, B., Phillips, N., & Schäfer, K. (1999). Survey and synthesis of intra-and interspecific variation in stomatal sensitivity to vapour pressure deficit. *Plant, Cell & Environment*, *22*, 1515–1526.

Osland, M. J., Feher, L. C., Griffith, K. T., Cavanaugh, K. C., Enwright, N. M., Day, R. H., et al. (2017). Climatic controls on the global distribution, abundance, and species richness of mangrove forests. *Ecological Monographs*, *87*, 341–359.

Reichstein, M., Falge, E., Baldocchi, D., Papale, D., Aubinet, M., Berbigier, P., et al. (2005). On the separation of net ecosystem exchange into assimilation and ecosystem respiration: Review and improved algorithm. *Global Change Biology*, *11*, 1424–1439.

Robertson, A. I., & Alongi, D. M. (2016). Massive turnover rates of fine root detrital carbon in tropical Australian mangroves. *Oecologia*, *180*, 841–851.

Sanders, C. J., Maher, D. T., Tait, D. R., Williams, D., Holloway, C., Sippo, J. Z., & Santos, I. R. (2016). Are global mangrove carbon stocks driven by rainfall? *Journal of Geophysical Research: Biogeosciences*, *121*, 2600–2609. https://doi.org/10.1002/2016JG00351

Shipley, B. (1997). Exploratory path analysis with applications in ecology and evolution. *The American Naturalist*, *149*, 1113–1138.

Simard, M., Fatoyinbo, L., Smetanka, C., Rivera-Monroy, V. H., Castañeda-Moya, E., Thomas, N., & Van Der Stocken, T. (2019). Mangrove canopy height globally related to precipitation, temperature and cyclone frequency. *Nature Geoscience*, *12*, 40–45.

Song, C., White, B. L., & Heumann, B. W. (2011). Hyperspectral remote sensing of salinity stress on red (*Rhizophora mangle*) and white (*Laguncularia racemosa*) mangroves on Galapagos Islands. *Remote Sensing Letters*, *2*, 221–230.

Takemura, T., Hanagata, N., Sugihara, K., Baba, S., Karube, I., & Dubinsky, Z. (2000). Physiological and biochemical responses to salt stress in the mangrove, *Bruguiera gymnorrhiza*. *Aquatic Botany*, *68*, 15–28.

Xu, D.-Q., & Shen, Y.-K. (1996). Midday depression of photosynthesis. In *Handbook of Photosynthesis* (pp. 451–459). CRC Press.

Ye, Y., Gu, Y., Gao, H., & Lu, C. (2010). Combined effects of simulated tidal sea-level rise and salinity on seedlings of a mangrove species, Kandelia candel (L.) Druce. *Hydrobiologia*, *641*, 287–300.

Zhu, X., Hou, Y., Weng, Q., & Chen, L. (2019). Integrating UAV optical imagery and LiDAR data for assessing the spatial relationship between mangrove and inundation across a subtropical estuarine wetland. *ISPRS Journal of Photogrammetry and Remote Sensing*, *149*, 146–156.

Zhu, X., Song, L., Weng, Q., & Huang, G. (2019). Linking in situ photochemical reflectance index measurements with mangrove carbon dynamics in a subtropical coastal wetland. *Journal of Geophysical Research: Biogeosciences*, *124*, 1714–1730. https://doi.org/10.1029/2019JG005022